ADVANCED MATERIALS
www.advmat.de

Exploring Electronic Characteristics of Acceptor–Donor–Acceptor-Type Molecules by Single-Molecule Charge Transport

Peihui Li, Wan Xiong, Jinying Wang, Jie Hao, Mingpeng Li, Boyu Wang, Yijian Chen, Wei Si, Haiyang Ren, Guangwu Li, Yongsheng Chen, Jingtao Lü, Hongtao Zhang,* Chuancheng Jia,* and Xuefeng Guo**

The electronic characteristics of organic optoelectronic materials determine the performance of corresponding devices. Clarifying the relationship between molecular structure and electronic characteristics at the single-molecule level can help to achieve high performance for organic optoelectronic materials and devices, especially for organic photovoltaics. In this work, a typical acceptor–donor–acceptor (A–D–A)-type molecule is explored by combining theoretical and experimental studies to reveal the intrinsic electronic characteristics at the single-molecule level. Specifically, the A–D–A-type molecule with 1,1-dicyano methylene-3-indanone (INCN) acceptor units exhibits an enhanced conductance in single-molecule junctions when compared with the control donor molecule, because the acceptor units of the A–D–A-type molecule contribute additional transport channels. In addition, through opening the S•••O noncovalent conformational lock by protonation to expose the −S anchoring sites, the charge transport of the D central part is detected, proving that the conductive orbitals contributed by the INCN acceptor groups can penetrate the whole A–D–A molecule. These results provide important insights into the development of high-performance organic optoelectronic materials and devices toward practical applications.

1. Introduction

The electronic characteristics of organic optoelectronic materials play a vital role in their optical, electrical and optoelectronic properties. Specifically, the molecular structure characteristics, including molecular geometry and conjugation degree,[1,2] determine the electronic characteristics. Therefore, establishing the relationship between molecular structure and electronic characteristics is helpful to further improve the performance of corresponding optoelectronic devices, including organic field-effect transistors,[3,4] organic light-emitting diodes[5] and organic photovoltaics.[6–8] In particular, among various types of organic photovoltaic materials, molecules with an acceptor–donor–acceptor (A–D–A) architecture have demonstrated considerable success in recent years.[2,9–13] At present, organic solar cells with high power conversion efficiency over 19% have been achieved,[8,14]

P. Li, J. Wang, J. Hao, B. Wang, Y. Chen, W. Si, H. Ren, G. Li, C. Jia, X. Guo
Center of Single-Molecule Sciences
Institute of Modern Optics
Frontiers Science Center for New Organic Matter
College of Electronic Information and Optical Engineering
Nankai University
38 Tongyan Road, Jinnan District, Tianjin 300350, P. R. China
E-mail: jiacc@nankai.edu.cn; guoxf@pku.edu.cn

W. Xiong, J. Lü
School of Physics
Institute for Quantum Science and Engineering and Wuhan National High Magnetic Field Center
Huazhong University of Science and Technology
Wuhan 430074, P. R. China
E-mail: jtlu@hust.edu.cn

J. Wang
Network for Computational Nanotechnology
Purdue University
West Lafayette, IN 47907, USA

M. Li, Y. Chen, H. Zhang
Center of Nanoscale Science and Technology and Key Laboratory of Functional Polymer Materials
Institute of Polymer Chemistry
College of Chemistry
Nankai University
Tianjin 300071, P. R. China
E-mail: htzhang@nankai.edu.cn

C. Jia, X. Guo
Beijing National Laboratory for Molecular Sciences
National Biomedical Imaging Center
College of Chemistry and Molecular Engineering
Peking University
292 Chengfu Road, Haidian District, Beijing 100871, P. R. China

The ORCID identification number(s) for the author(s) of this article can be found under https://doi.org/10.1002/adma.202301876

DOI: 10.1002/adma.202301876

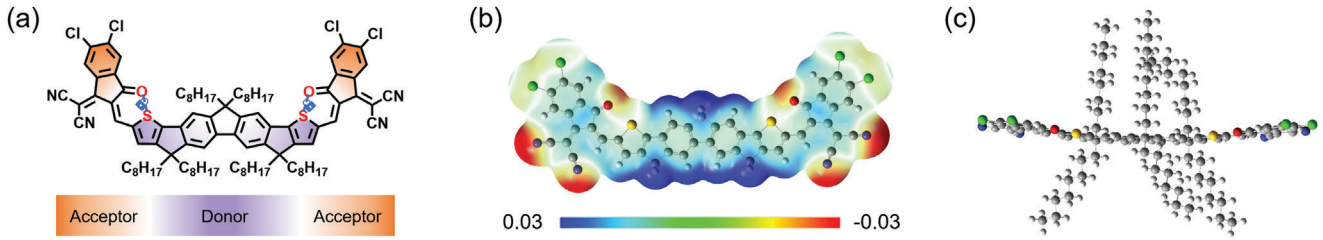

Figure 1. Design of the A–D–A molecule. a) Chemical structure of the designed A–D–A molecule. b) Calculated electrostatic potential mapping of the A–D–A molecule without branched alkanes. The blue color represents the positive charge, while the red color represents the negative charge. ESP unit: Hartree/e. c) Theoretical optimized molecular structure of the A–D–A molecule.

in which A–D–A-type molecules act as acceptor materials in the mixture active layer. Since the electronic characteristics of A–D–A-type molecules determine the light absorption, exciton separation, and charge transportation in the photovoltaic process, it is crucial to explore the molecular electronic characteristics at the single-molecule level, especially the role of bilateral A groups.

Single-molecule junction technologies,[15] such as mechanically controllable break junction, scanning tunneling microscopy break junction (STM-BJ), and lithography-defined single-molecule junction, can connect a single molecule between two electrodes for charge-transport measurements. Because molecular electronic characteristics, including molecular orbital energy levels,[16,17] orbital density of states, and electrostatic potential distribution,[15] determine the charge-transport properties of single molecules, these electronic characteristics can be concluded by single-molecule electrical study. For the most commonly used A–D–A-type molecules in high-performance organic photovoltaic devices, they usually have fused backbone D units and 1,1-dicyano methylene-3-indanone (INCN) or its derivatives as the end groups.[2] Here, single-molecule charge-transport characteristics of a typical A–D–A-type F2Cl molecule[11] (A–D–A for short) with chlorinated INCN acceptor groups and a thiophene-fused fluorene donor central block were studied by the STM-BJ technology (Figures S1 and S2, Supporting Information). Using thiophene-fused fluorene donor molecule (D for short) as a control, the effect of INCN acceptor groups on the electronic characteristics of A–D–A molecules was explored by single-molecule charge-transport analysis. In addition, through opening the S•••O noncovalent conformational lock by protonation to expose the −S anchoring sites, the charge transport of the D center part was directly measured, clarifying the effect of INCN acceptor groups on electronic characteristics of the D center.

2. Results and Discussion

2.1. Design of the A–D–A Molecule

Based on the concept of molecular engineering, an A–D–A-type F2Cl molecule with chlorinated INCN acceptor groups on both sides and a thiophene-fused fluorene central donor unit was synthesized (**Figure 1**a; Figure S3–1a, Supporting Information).[11] Due to the electron withdrawing effect of the chlorinated INCN acceptor unit and the electron donating effect of the thiophene-fused fluorene donor unit, the charge distribution on the molecule is uneven, which can be confirmed by calculated electrostatic potential mapping (Figure 1b) and be consistent with other molecules with the A–D–A architecture.[18] The special charge distribution feature would affect the charge transport and promote the charge separation of the molecule. Meanwhile, this A–D–A molecule has an interesting S•••O noncovalent conformational lock with a Mayer bond order of ≈0.08 and a bond length of ≈2.695 Å (Figures S4 and S5, Supporting Information). This noncovalent through-space intramolecular interactions between −S and −O sites can restrict the rotation around the single bonds between the acceptor groups and the donor center group. Therefore, the planarity and rigidity of the molecule will increase (Figure 1c), which is beneficial to extend the π-electron system.

2.2. Exploring Electronic Characteristics of a Single A–D–A Molecule and Control D Molecule

To study the electronic characteristics, the charge transport of a single A–D–A molecule and control molecule only with the donor unit (Figure S3–1b, Supporting Information) were measured by the STM-BJ technology that forms dynamic single-molecule junctions (**Figure 2**a,d). Specifically, single-molecule conductance is repeatedly measured as a function of tip-substrate displacement to generate conductance versus displacement traces by the STM-BJ technique. The single-molecule junctions are formed and broken in the solution of 1,2,4-trichlorobenzene (TCB) containing the target molecule of 0.1 mM. Typical individual traces for A–D–A junctions under 0.1 V bias are presented as yellow lines in Figure 2b and Figure S6 (Supporting Information). The conductance features at integer multiples of G_0 ($G_0 = 2e^2/h$) and the features below G_0 at specific molecular values can be observed. The purple traces show the tunnelling decay after the rupture of an Au atomic contact in pure solvent (Figures S6 and S7, Supporting Information), while the conductance plateaus corresponding to the molecular conductance could be found in the solution with target molecules. Thousands of such conductance traces are used to construct conductance histograms. Figure 2b presents the 2D conductance–displacement histogram of the A–D–A molecule. A Gaussian fitting conductance peak can be observed at $\approx 1.3 \times 10^{-4}$ G_0 (≈10.08 nS). Since the −S sites are locked by the S•••O interactions, this conductance is attributed to the charge transport through the −CN anchors of INCN acceptor groups on both sides of the molecule, not the carbonyl site (Figure S8, Supporting Information). While for the control donor type molecule D, a similar conductance peak at $\approx 5.0 \times 10^{-5}$ G_0 (≈3.9 nS) can be observed (Figure 2d–f; Figure S9, Supporting

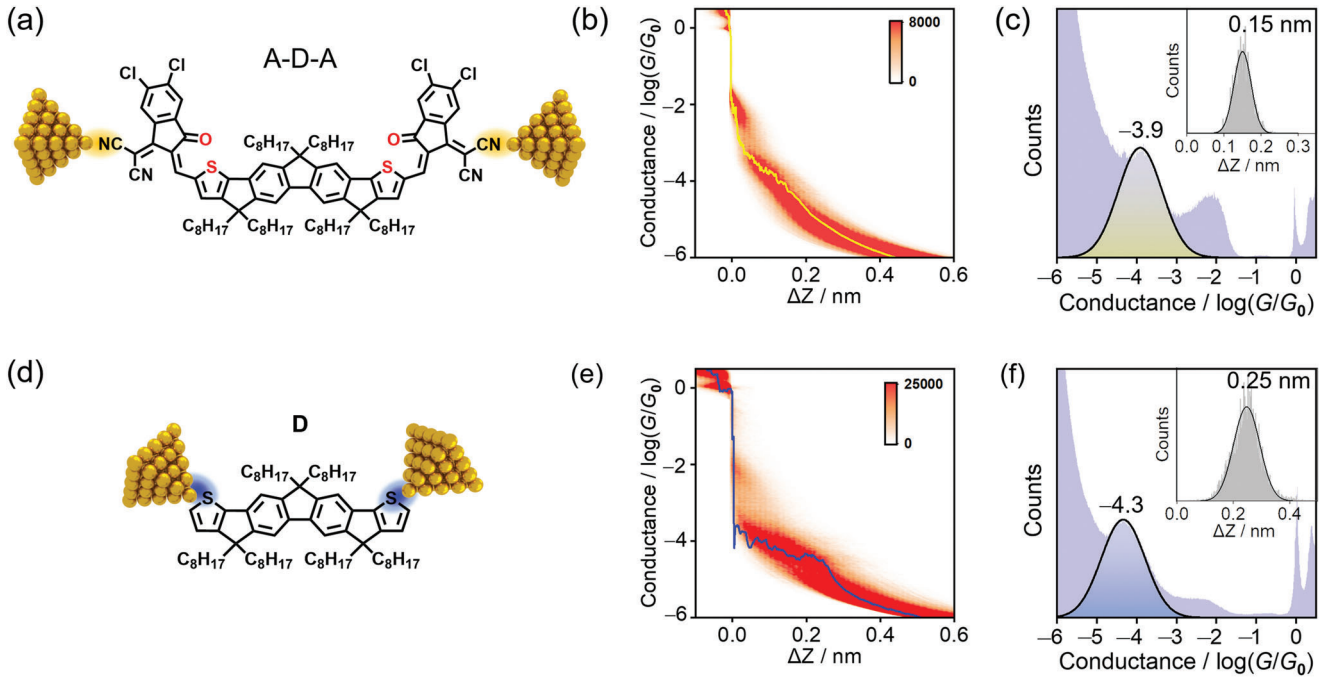

Figure 2. Single-molecule electrical measurements of A–D–A and D molecules. a,d) Schematic of STM-BJ measurements of a single A–D–A molecule junction (a) and a single D molecule junction (d). b,e) The 2D conductance–displacement histograms for A–D–A junctions (b) and D junctions (e). The color bar indicates the number of counts. The typical single trace is marked. c,f) The 1D conductance histograms of A–D–A junctions (c) and D junctions (f). Inset: the corresponding relative stretching distance distributions of molecular junctions.

Information). In addition, the plateau length of the A–D–A junction is shorter than that of the D junction during the stretching process (the insert in Figure 2c,f), indicating that the A–D–A junction is easier to break. Since the binding energy between Au and −CN (≈0.50 eV) is weaker than that between Au and −S (≈0.67 eV),[19] it is reasonable that the charge transport of the A–D–A molecule is through −CN sites. It is worth mentioning that though the transport pathway of A–D–A is longer than D, the conductance of A–D–A is higher than that of D, which is contrary to the general situation (Figure S10, Supporting Information).[20–22]

To further explore the charge transport of single-molecule junctions, the current versus voltage (I–V) and conductance versus voltage ($\mathrm{d}I/\mathrm{d}V$–V) characteristics were investigated. It is worth noting that the $\mathrm{d}I/\mathrm{d}V$ is calculated from the I/V data obtained from experiments by the derivative calculation. Specifically, the I–V characterizations were implemented by holding the gold tip when the corresponding conductance plateau is formed during the break junction measurement and scanning the bias voltage from −1.0 to 1.0 V with a step of 0.0005 V. The collected I–V traces were used to construct 2D I–V histograms. **Figure 3**a and Figure 3d show the 2D I–V histograms of A–D–A and D junctions, respectively, while Figure 3b and Figure 3e present the corresponding 2D $\mathrm{d}I/\mathrm{d}V$–V histograms. From the 2D $\mathrm{d}I/\mathrm{d}V$–V histograms, it can be observed that the conductance of A–D–A is higher than that of donor type molecule D, especially at small bias voltage, which is consistent with the above (Figure 2b,e). When the bias voltage increases, the conductance of both D junctions and A–D–A junctions increase. The difference is that the conductance growth rate of the D junction with the increase of the bias voltage is from slow to fast, while that of the A–D–A junction is from fast to slow (Figure S11, Supporting Information). This indicates that the conductive orbitals of the two molecules entering the bias window are different. To better understand this case, the transition voltage spectra (TVS) is analyzed, which refers to the Fowler–Nordheim plot ($\ln(I/V^2)$ versus $1/V$). Specifically, the position of the minimum in the TVS, called the transition voltage (V_{trans}), is related to the energy level difference between the closest molecular orbital and the Fermi level of the electrodes.[23,24] Since the I–V characteristics are symmetrical for all conductance states (Figure S12, Supporting Information), this symmetric feature is also reflected in the results of the corresponding TVS (Figure 3c,f). Through comparing the V_{trans} values between A–D–A and D junctions, it is observed that the absolute V_{trans} value of the D junction is smaller than that of the A–D–A junction, which is ≈0.5 V and 0.7 V, respectively.

From theoretical transmission spectra, it is found that the conductance of the A–D–A molecule (Figure S13b, Supporting Information) through the −CN (in acceptor unit) anchored way near the Fermi energy is higher than that of the donor type molecule D (Figure S13a, Supporting Information) through the −S anchored way (Figure 3g), which is consistent with experimental results. It is worth noting that the structural parameters of the A–D–A molecule in the transmission spectra calculation are consistent with the single-crystal data (Figure S4, Supporting Information).[25,26] In addition, in comparison with the D junction, the A–D–A junction possesses additional transport molecular orbitals between the original perturbed highest occupied molecular orbital (p-HOMO) and the perturbed lowest unoccupied molecular orbital (p-LUMO) of the D molecule (Figure S14, Supporting Information), which is supposed to originate from

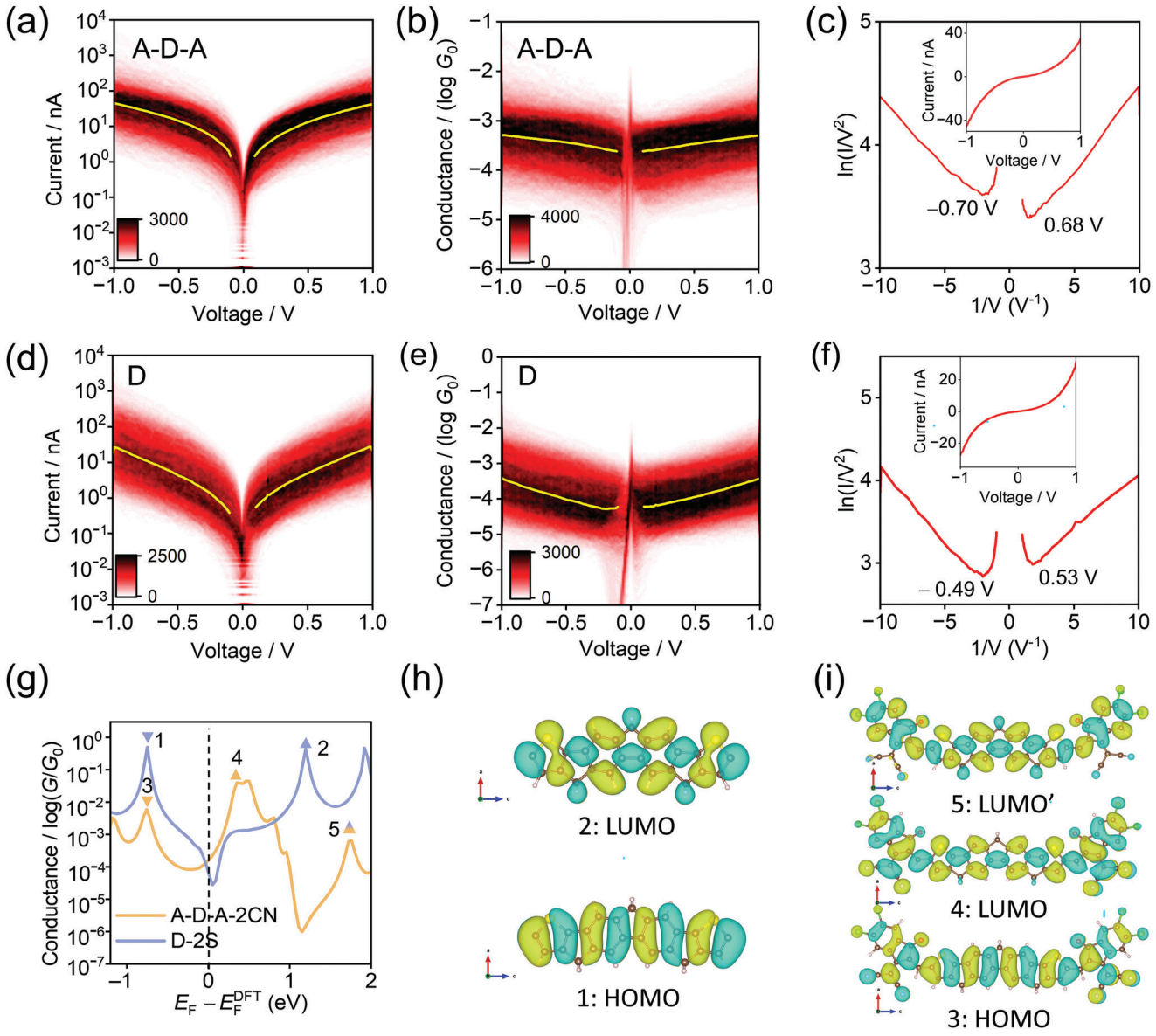

Figure 3. Comparison of the charge-transport and electronic characteristics between single A–D–A and D junctions. a,d) The 2D current versus voltage (*I–V*) histograms of A–D–A junctions (a) and D junctions (d). b,e) The 2D conductance versus voltage (d*I*/d*V*–*V*) histograms of A–D–A junctions (b) and (D junctions e). The yellow line represents the most representative current value from the Gaussian fitting. c,f) Fowler–Nordheim plots constructed from the corresponding fitted *I–V* curves (yellow line) in (a) and (d), respectively. The transition voltages for positive and negative polarities were marked out. The insets show the corresponding *I–V* curve on a linear scale. g) Calculated transmission spectra of the A–D–A junction (yellow) and the D junction (purple). The triangles mark out the position of the transmission peaks corresponding to the intrinsic molecular orbitals. The downward represents HOMO and upward represents LUMO. The gradient triangle marks out LUMO' of molecule D. The dotted line represents the Fermi energy level of electrodes. h,i) Calculated molecular orbital diagrams for molecule D (h) and molecule A–D–A (i). The numbers (1, 2, 3, 4, and 5) represent the different molecular orbitals that mainly determine the position of the conductive peaks marked in (g).

the acceptors, inducing the nonclassical higher conductance of the A–D–A junction than the D junction (Figure S15, Supporting Information). Specifically, the simulated molecular orbital diagrams of molecule D (LUMO and HOMO) and molecule A–D–A (LUMO' and HOMO) show that the central part of A–D–A has the same orbital characteristics with D (Figure 3h,i). It is worth mentioning that the newly appeared additional LUMO orbitals of the A–D–A molecule possess excellent conjugation between the donor center and acceptor groups on both sides, leading to the excellent charge-transport properties of the A–D–A molecule (Figure S16–1, Supporting Information).

2.3. Exploring the Effect of INCN Acceptor on Electronic Characteristics of the Donor Center

To better understand the effect of bilateral INCN acceptor groups on electronic characteristics of the D center, it is necessary to

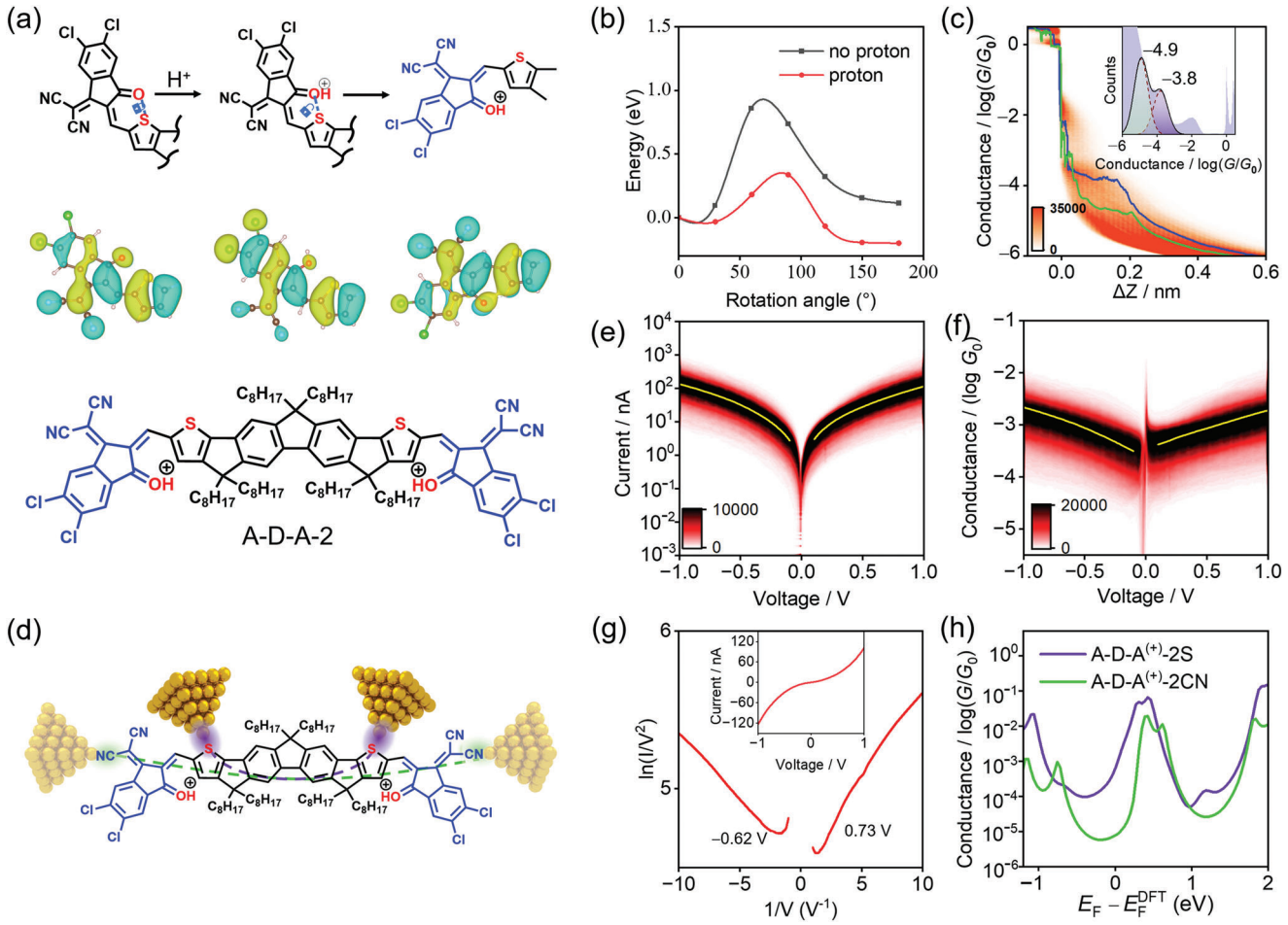

Figure 4. Effect of the INCN acceptor on electronic characteristics of the donor center after molecule protonation. a) Schematic illustration of the effect of protonation on intramolecular S•••O conformational lock and molecular structures. b) Calculated conformational inversion barriers for A–D–A with (red) or without (black) protonation. c) The 2D conductance–displacement histogram for A–D–A junctions after protonation. The purple line and green line are typical single traces for high and low conductance states, respectively. Inset: corresponding 1D conductance histograms. d) Schematic illustration of single-molecule junctions for the A–D–A–2 structure by different anchor groups. e,f) The 2D *I*–*V* histograms (e) and 2D d*I*/d*V*–*V* histograms (f) of A–D–A junctions after protonation. The yellow line represents the most representative current value from the Gaussian fitting. g) Fowler–Nordheim plots constructed from the corresponding fitted *I*–*V* curves (yellow line) in (e). The insets show the corresponding *I*–*V* curve on a linear scale. h) Calculated transmission spectra of A–D–A–2 through −S (purple) and −CN (green).

directly detect the charge transport of the D central part. Since the −S sites in the A–D–A molecule are locked by an intramolecular S•••O noncovalent conformational lock,[27,28] the proton is introduced to regulate the S•••O noncovalent conformational lock and corresponding molecular structure. Specifically, the proton that can bond with oxygen atom will affect the S•••O noncovalent intramolecular interaction, and further cause the conformation reversion of the A–D–A molecule (**Figure 4**a). In particular, according to the theoretical optimization, it is found that the proton tends to bond with oxygen. Based on it, the theoretical results show the conformation inversion barrier for the A–D–A molecule decreases from ≈1.0 to ≈0.35 eV without and with protonation, respectively (Figure 4b). Furthermore, the energy of the reverse-turn conformation is lower than that of the original conformation, indicating that the protonated molecule will mainly be in the reverse conformation (A–D–A–2). Therefore, with the proton bonding and conformation inversion, the −S sites at the D center will be exposed, which can be used to further connect the external electrodes.

To investigate the charge-transport characteristics of the A–D–A molecule with protonation, the STM-BJ experiments have been carried out with adding trifluoroacetic acid (TFA) to the solution containing the target molecules. From the 2D conductance histogram (Figure 4c), it can be observed that two conductance peaks appear at ≈1.3×10^{-5} G_0 (≈1.0 nS) and ≈1.6×10^{-4} G_0 (≈12.3 nS). The plateau length of high conductance state is longer than that of the A–D–A molecule without TFA treatment, indicating that the binding energy of new anchors and gold electrodes is stronger than that without protonation. Because the binding energy of −S and Au is stronger than that of −CN and Au, the high conductance state is assumed to originate from the −S anchoring way (Figure 4d). To verify this assumption, the *I*–*V* characteristics of the high conductance state are explored by the STM-BJ experiment. From the corresponding 2D *I*–*V* histogram and 2D

dI/dV–V histograms, it can be observed that the conductance of the protonated A–D–A molecule is higher than that of A–D–A without protonation (Figure 4e,f). In addition, with the increase of bias voltage, the conductance of the protonated A–D–A junction increases faster than that of the A–D–A junction without protonation. This may be due to the fact that the opposite dipole moments between the donor and bilateral acceptors could generate double barriers along the charge-transport channel of the A–D–A junction with –CN anchoring sites, which suppress the bias-dependent charge transport.[29] All these support that the high conductance state should originate from the −S anchoring way, which becomes feasible after proton bonding and conformation inversion. It is worth mentioning that the TVS characteristics of protonated A–D–A is closer to that of A–D–A without protonation, whose absolute V_{trans} value is also at 0.6 V–0.7 V (Figure 4g). This is because even though the protonation causes the conformation inversion, the orbital energy level characteristics change little, which can be confirmed from the calculated transmission spectra of protonated A–D–A through different anchoring ways (Figure 4h). From the theoretical molecular orbital diagrams (Figure S16–2, Supporting Information), it can be observed that when the charge transport is through the −S sites, the acceptors contribute additional transport molecular orbitals to the central part. Furthermore, even if the INCN acceptor is replaced by an acceptor without the noncovalent conformation lock, it can be observed that the acceptor also contributes additional transport molecular orbitals to the central part (Figure S17, Supporting Information).

From the theoretically calculated conductance through −CN sites and −S sites, it can be determined that the high conductance state comes from the −S anchoring way and the low conductance state comes from the −CN anchoring way (Figure 4h). It should be emphasized that the conductance through the −CN anchoring way of protonated A–D–A is lower than that of A–D–A without protonation, which is due to the decrease of the conjugation of the A–D–A molecule after the reversion induced by protonation (Figure S18, Supporting Information). To exclude other possible cases, especially the case of proton bonding to −S or −CN sites, the control experiments were conducted. Specifically, the 7,7,8,8-tetracyanoquinodimethane (TCNQ) molecule with −CN anchoring groups was measured by STM-BJ without and with TFA treatment. The results show that the conductance has almost no change, proving that the proton is not bonded with −CN to cause the conductance change (Figure S19, Supporting Information). For the D molecule without acceptor units (A units), the results show that the conductance of the D junction treated with TFA is almost the same as that without TFA treatment (Figure 2e,f; Figure S20, Supporting Information), supporting proton bonding with oxygen rather than sulfur.

3. Conclusion

The electronic characteristics of a A–D–A-type molecule were investigated by combining dynamic single-molecule junction electrical measurements and theoretical simulation analysis. Specifically, it is found that the A–D–A molecule have higher conductance than the D molecule with a shorter molecular length. In combination with theoretical simulation, it can be proved that due to the effective orbital hybridization of the central donor unit with ending acceptor groups on both sides, additional transport molecular orbitals appear in the middle of the energy gap, leading to the nonclassical high conductance of the A–D–A molecule in the junction. In addition, the −S anchoring sites are exposed by opening the S•••O noncovalent conformational lock through protonation, so the charge transport of the D central part can be directly detected, proving that the conductive orbitals contributed by the INCN acceptor groups could penetrate the whole A–D–A molecule. Understanding these electronic characteristics of A–D–A-type molecules from the single-molecule electrical perspective, especially the role of acceptor groups in A–D–A-type molecules (Figure S21, Supporting Information), can provide deep insights into the design of A–D–A-type molecules with flexible capability of regulation to construct high-performance electronic/optoelectronic devices. In particular, photovoltaic materials are expected to be designed more effectively under the guidance of single-molecule charge transfer and orbital analysis.

4. Experimental Section

Materials and Characterizations: Gold wire (99.99%, 0.25 mm diameter) was purchased from ZhongNuo Advanced Material (Beijing) Technology Co., Ltd. for the fabrication of the STM tip. The gold tip was obtained by electrochemical corrosion. Substrates were prepared by depositing 10 nm thick chromium film and 200 nm thick gold film on the monocrystalline face of silicon wafers. The target molecules were dissolved in TCB solvent (0.1 mM). The UV–vis absorption spectra were measured on a UV–vis spectrophotometer (Agilent Cary 60).

STM-BJ Measurements: In the STM-BJ measurements, the distance between the gold tip and the substrate was controlled by a stepper motor and a piezo stack. The bias voltage was applied between the tip and the substrate, and the current was used as the feedback to control the movement of the gold tip. During the repeated tip retracting and tip approaching cycles, the conductance versus displacement traces are collected, and the traces of the tip approaching cycles were used for further analysis. All measurements were carried out at room temperature. The single-molecule conductance measurements were carried out using Xtech STMBJ developed by Prof. Wenjing Hong's group in Xiamen University, and the data was analyzed by XMe open-source code (https://github.com/Pilab-XMU/XMe_DataAnalysis).

I–V Characterizations: The *I–V* characterizations were carried out by the methods developed from previous studies.[30,31] An automated control program running on an NI cRIO-9039 controller was used, and the plateau was determined through the judgement in the control program. The judgement detects the sampling points within a preset conductance range, which was determined by referring to the statistical conductance range of the target molecule. If the sampling points within this range exceed a certain threshold, it means that there was a conductance plateau emerged. At this time, the movement of the piezo was paused to keep the molecular junction in such a conductance range. When this happens, the measurement mode is switched to *I–V* measurement, which is completed within 150 ms during the experiments. After the *I–V* measurement, the control program is automatically switched to the current–time curve measurement mode. If the measured conductance is still within the preset conductance range, the measured *I–V* curve is collected for the subsequent statistical analysis. Otherwise, the *I–V* curve will be rejected by the control program. The 2D *I–V* histograms were plotted in a 200 × 200 array, and the Gaussian fitting in each column of the array was used to obtain the fitting line. Finally, the transition voltage spectrum from the above fitting line is plotted according to the previous studies.[32] The *I–V* curves in the 2D *I–V* histograms remain unchanged, as they were collected from the *I–V* measurements.

Theoretical Calculations: First principles calculations of isolated molecules were performed based on the density functional theory (DFT)

as implemented in the Vienna Ab initio Simulation Package (VASP). The ion-electron interaction was described with the projector augmented wave (PAW) method. The cutoff energy of 400 eV was used for the plane-wave basis set. An electron exchange–correlation effect was described using the generalized gradient approximation (GGA) of the Perdew–Burke–Ernzerhof (PBE) functional. All atoms were relaxed until the force was less than 0.02 eV $Å^{-1}$. The criterion for the total energy was set as 1×10^{-5} eV. The climbing image–nudged elastic band (CI-NEB) method calculations [33,34] were performed to find the minimum energy pathways and energy barriers for transformation among different structure. An electrode–central region–electrode junction setup was used for the DFT–NEGF calculations, as exemplified with A–D–A. The respective electrodes extend semi-infinitely to either side in the calculations. Au (100) surface (AB-stacking) 8*4*1 supercell was utilized as the electrode (128 atoms) and central region consists of the molecule and some adjacent Au atoms, as shown in Figure S22 (Supporting Information). In particular, when the size (number of atomic layers) of the electrodes changes from 4 to 8 layers, there is almost no effect on the transmission of the junction (Figure S23, Supporting Information). Next, to get optimized junctions' structures, SIESTA was used and the same parameters with the previous structure relaxation were chosen (Figure S24, Supporting Information). For each structure, the transmission coefficient $T(E)$ describing the propagation of electrons of the energy E from the left electrode to the right one is obtained via an ab initio non-equilibrium Green's function (NEGF) approach based on density functional theory (DFT), as implemented in the TranSIESTA[35,36] and TBtrans. Throughout the TranSIESTA calculation, a single-ζ plus polarization (SZP) basis set was used. To converge the total energy, the cutoff energy was set to 100 Ry.

Supporting Information

Supporting Information is available from the Wiley Online Library or from the author.

Acknowledgements

The authors acknowledge primary financial supports from the National Key R&D Program of China (2021YFA1200102, 2021YFA1200101, and 2022YFE0128700), the National Natural Science Foundation of China (22173050, 22150013, 21727806, and 21933001), the Fundamental Research Funds for the Central Universities (63223056 and 63223054), the Tencent Foundation through the XPLORER PRIZE, "Frontiers Science Center for New Organic Matter" at Nankai University (63181206), the Natural Science Foundation of Beijing (2222009) and Beijing National Laboratory for Molecular Sciences (BNLMS202105).

Conflict of Interest

The authors declare no conflict of interest.

Author Contributions

P.L., W.X., J.W., and J.H. contributed equally to this work. X.G., C.J., and H.Z. conceived the idea for the paper. P.L. and Y.J.C. carried out the experimental measurements. Y.S.C., H.Z., and M.L. carried out the molecular synthesis. J.L., W.X., J.W., and J.H. built and analyzed the theoretical model and performed the quantum transport calculation. P.L. draw the diagrams. X.G., C.J., P.L., W.X., B.W., H.R., W.S., and G.L. analyzed the data and wrote the paper. All the authors discussed the results and commented on the manuscript.

Data Availability Statement

The data that support the findings of this study are available from the corresponding author upon reasonable request.

Keywords

A–D–A molecules, charge transport, noncovalent conformational locks, single-molecule junctions

Received: February 27, 2023
Revised: March 30, 2023
Published online: May 30, 2023

[1] L. Ye, K. Weng, J. Xu, X. Du, S. Chandrabose, K. Chen, J. Zhou, G. Han, S. Tan, Z. Xie, Y. Yi, N. Li, F. Liu, J. M. Hodgkiss, C. J. Brabec, Y. Sun, *Nat. Commun.* **2020**, *11*, 6005.
[2] X. J. Wan, C. X. Li, M. T. Zhang, Y. S. Chen, *Chem. Soc. Rev.* **2020**, *49*, 2828.
[3] P. Li, C. Jia, X. Guo, *Chem. Rec.* **2021**, *21*, 1284.
[4] L. Meng, N. Xin, C. Hu, H. A. Sabea, M. Zhang, H. Jiang, Y. Ji, C. Jia, Z. Yan, Q. Zhang, L. Gu, X. He, P. Selvanathan, L. Norel, S. Rigaut, H. Guo, S. Meng, X. Guo, *Nat. Commun.* **2022**, *13*, 1410.
[5] Y. Xu, P. Xu, D. Hu, Y. Ma, *Chem. Soc. Rev.* **2021**, *50*, 1030.
[6] P. Li, Y. Chen, B. Wang, M. Li, D. Xiang, C. Jia, X. Guo, *Opto-Electron. Adv.* **2022**, *5*, 210094.
[7] Y. Jiang, X. Dong, L. Sun, T. Liu, F. Qin, C. Xie, P. Jiang, L. Hu, X. Lu, X. Zhou, W. Meng, N. Li, C. J. Brabec, Y. Zhou, *Nat. Energy.* **2022**, *7*, 352.
[8] L. Zhu, M. Zhang, J. Xu, C. Li, J. Yan, G. Zhou, W. Zhong, T. Hao, J. Song, X. Xue, Z. Zhou, R. Zeng, H. Zhu, C. C. Chen, R. C. I. MacKenzie, Y. Zou, J. Nelson, Y. Zhang, Y. Sun, F. Liu, *Nat. Mater.* **2022**, *21*, 656.
[9] C. Jiao, Z. Guo, B. Sun, Y. Yi, L. Meng, X. Wan, M. Zhang, H. Zhang, C. Li, Y. Chen, *J Mater Chem* **2020**, *8*, 6293.
[10] Y. Zhang, H. Feng, L. Meng, Y. Wang, M. Chang, S. Li, Z. Guo, C. Li, N. Zheng, Z. Xie, X. Wan, Y. Chen, *Adv. Energy Mater.* **2019**, *9*, 1902688.
[11] Y. Wang, Y. Wang, B. Kan, X. Ke, X. Wan, C. Li, Y. Chen, *Adv. Energy Mater.* **2018**, *8*, 1802021.
[12] L. X. Meng, Y. M. Zhang, X. J. Wan, C. X. Li, X. Zhang, Y. B. Wang, X. Ke, Z. Xiao, L. M. Ding, R. X. Xia, H. L. Yip, Y. Cao, Y. S. Chen, *Science* **2018**, *361*, 1094.
[13] H. Gao, C. Han, X. Wan, Y. Chen, *Ind. Chem. Mater.* **2023**, *1*, 60.
[14] K. Chong, X. Xu, H. Meng, J. Xue, L. Yu, W. Ma, Q. Peng, *Adv. Mater.* **2022**, *34*, 2109516.
[15] P. Li, L. Zhou, C. Zhao, H. Ju, Q. Gao, W. Si, L. Cheng, J. Hao, M. Li, Y. Chen, C. Jia, X. Guo, *Rep Prog Phys* **2022**, *85*, 086401.
[16] Y. Li, M. Buerkle, G. Li, A. Rostamian, H. Wang, Z. Wang, D. R. Bowler, T. Miyazaki, L. Xiang, Y. Asai, G. Zhou, N. Tao, *Nat. Mater.* **2019**, *18*, 357.
[17] J. Liu, X. Huang, F. Wang, W. Hong, *Acc. Chem. Res.* **2019**, *52*, 151.
[18] M. Ans, F. Manzoor, K. Ayub, F. Nawaz, J. Iqbal, *J. Mol. Model.* **2019**, *25*, 222.
[19] C. Jia, X. Guo, *Chem. Soc. Rev.* **2013**, *42*, 5642.
[20] S. H. Choi, B. Kim, C. D. Frisbie, *Science* **2008**, *320*, 1482.
[21] T. Hines, I. Diez-Perez, J. Hihath, H. M. Liu, Z. S. Wang, J. W. Zhao, G. Zhou, K. Muellen, N. J. Tao, *J. Am. Chem. Soc.* **2010**, *132*, 11658.
[22] Y. Li, H. Wang, Z. Wang, Y. Qiao, J. Ulstrup, H. Y. Chen, G. Zhou, N. Tao, *Proc. Natl. Acad. Sci. USA* **2019**, *116*, 3407.
[23] A. Feng, Y. Zhou, M. A. Y. Al-Shebami, L. Chen, Z. Pan, W. Xu, S. Zhao, B. Zeng, Z. Xiao, Y. Yang, W. Hong, *Nat. Chem.* **2022**, *14*, 1158.
[24] J. M. Beebe, B. Kim, J. W. Gadzuk, C. D. Frisbie, J. G. Kushmerick, *Phys. Rev. Lett.* **2006**, *97*, 026801.
[25] W. Zhu, A. P. Spencer, S. Mukherjee, J. M. Alzola, V. K. Sangwan, S. H. Amsterdam, S. M. Swick, L. O. Jones, M. C. Heiber, A. A. Herzing, G. Li, C. L. Stern, D. M. DeLongchamp, K. L. Kohlstedt, M. C. Hersam,

G. C. Schatz, M. R. Wasielewski, L. X. Chen, A. Facchetti, T. J. Marks, *J. Am. Chem. Soc.* **2020**, *142*, 14532.
[26] G. Zhang, X. K. Chen, J. Xiao, P. C. Y. Chow, M. Ren, G. Kupgan, X. Jiao, C. C. S. Chan, X. Du, R. Xia, Z. Chen, J. Yuan, Y. Zhang, S. Zhang, Y. Liu, Y. Zou, H. Yan, K. S. Wong, V. Coropceanu, N. Li, C. J. Brabec, J. L. Bredas, H. L. Yip, Y. Cao, *Nat. Commun.* **2020**, *11*, 3943.
[27] H. Huang, L. Yang, A. Facchetti, T. J. Marks, *Chem. Rev.* **2017**, *117*, 10291.
[28] Y. Che, M. R. Niazi, R. Izquierdo, D. F. Perepichka, *Angew. Chem., Int. Ed.* **2021**, *60*, 24833.
[29] M. Li, H. Fu, B. Wang, J. Cheng, W. Hu, B. Yin, P. Peng, S. Zhou, X. Gao, C. Jia, X. Guo, *J. Am. Chem. Soc.* **2022**, *144*, 20797.
[30] B. Capozzi, J. Xia, O. Adak, E. J. Dell, Z. F. Liu, J. C. Taylor, J. B. Neaton, L. M. Campos, L. Venkataraman, *Nat. Nanotechnol.* **2015**, *10*, 522.
[31] G. Lovat, B. Choi, D. W. Paley, M. L. Steigerwald, L. Venkataraman, X. Roy, *Nat. Nanotechnol.* **2017**, *12*, 1050.
[32] E. H. Huisman, C. M. Guedon, B. J. van Wees, S. J. van der Molen, *Nano Lett.* **2009**, *9*, 3909.
[33] G. Henkelman, B. P. Uberuaga, H. Jonsson, *J. Chem. Phys.* **2000**, *113*, 9901.
[34] V. Asgeirsson, B. O. Birgisson, R. Bjornsson, U. Becker, F. Neese, C. Riplinger, H. Jonsson, *J. Chem. Theory Comput.* **2021**, *17*, 4929.
[35] N. Papior, N. Lorente, T. Frederiksen, A. García, M. Brandbyge, *Comput. Phys. Commun.* **2017**, *212*, 8.
[36] M. Brandbyge, J.-L. Mozos, P. Ordejón, J. Taylor, K. Stokbro, *Phys. Rev. B* **2002**, *65*, 165401.